

SD-CNN: a Shallow-Deep CNN for Improved Breast Cancer Diagnosis

Fei Gao, Teresa Wu, Jing Li, *Member, IEEE*, Bin Zheng, Lingxiang Ruan, Desheng Shang and Bhavika Patel

Abstract—Breast cancer is the second leading cause of cancer death among women worldwide. Nevertheless, it is also one of the most treatable malignances if detected early. Screening for breast cancer with digital mammography (DM) has been widely used. However it demonstrates limited sensitivity for women with dense breasts. An emerging technology in the field is contrast-enhanced digital mammography (CEDM), which includes a low energy (LE) image similar to DM, and a recombined image leveraging tumor neoangiogenesis similar to breast magnetic resonance imaging (MRI). CEDM has shown better diagnostic accuracy than DM. While promising, CEDM is not yet widely available across medical centers. In this research, we propose a Shallow-Deep Convolutional Neural Network (SD-CNN) where a shallow CNN is developed to derive “virtual” recombined images from LE images, and a deep CNN is employed to extract novel features from LE, recombined or “virtual” recombined images for ensemble models to classify the cases as benign vs. cancer. To evaluate the validity of our approach, we first develop a deep-CNN using 49 CEDM cases collected from Mayo Clinic to prove the contributions from recombined images for improved breast cancer diagnosis (0.86 in accuracy using LE imaging vs. 0.90 in accuracy using both LE and recombined imaging). We then develop a shallow-CNN using the same 49 CEDM cases to learn the nonlinear mapping from LE to recombined images. Next, we use 69 DM cases collected from the hospital located at Zhejiang University, China to generate “virtual” recombined images. Using DM alone provides 0.91 in accuracy, whereas SD-CNN improves the diagnostic accuracy to 0.95.

Index Terms— Deep learning, Image reconstruction, Breast Tumor, Digital mammography, Diagnosis

I. INTRODUCTION

Although about 1 in 8 U.S. women (~12%) will develop invasive breast cancer over the course of her lifetime [1], breast cancer death rates have been steadily and/or significantly

decreasing since the implementation of the population-based breast cancer screening program in late 1970s due to the early cancer detection and the improved cancer treatment methods [2]. Among the existing imaging modalities, digital mammography (DM) is the only clinically acceptable imaging modality for the population-based breast cancer screening, while Ultrasound (US) and Magnetic Resonance Imaging (MRI) are also used as adjunct imaging modalities to mammography for certain special subgroups of women [3]. However, using DM is not an optimal approach in breast cancer screening due to its relatively low detection sensitivity in many subgroups of women. For example, although DM screening has an overall cancer detection sensitivity of 0.75 to 0.85 in the general population, its sensitivity in several subgroups of the high-risk women including those with positive BRCA (BRest CAncer) mutation or dense breasts decreases to 0.30 to 0.50 [4][5]. On the other hand, using dynamic contrast enhanced breast MRI can yield significantly higher cancer detection sensitivity due to its ability to detect tumor angiogenesis through contrast enhancement [6][7]. Yet, its substantially higher cost, lower accessibility and longer imaging scanning time forbids breast MRI being used as a primary imaging modality in breast cancer screening and detection. In addition, lower image resolution of breast MRI is a disadvantage as comparing to DM.

In order to combine the advantages of both DM and MRI, a new novel imaging modality namely, contrast-enhanced digital mammography (CEDM) emerges and starts to attract broad research and clinical application interest. CEDM includes low energy (LE) imaging, which is similar to DM, and recombined imaging similar to breast MRI. Comparing to breast MRI, CEDM exam is about 4 times faster with only about 1/6 the cost [8]. In addition, CEDM imaging has 10 times the spatial resolution of breast MRI. As a result, CEDM can be used to more sensitively detect small residual foci of tumor, including calcified Ductal Carcinoma in Situ (DCIS), than using MRI [8]. Several studies including prospective clinical trials conducted at Mayo Clinic have indicated that CEDM is a promising imaging modality that overcomes tissue overlapping (“masking”) occurred in DM, provides tumor neovascularity related functional information similar to MRI, while maintaining high image resolution of DM [9]-[12]. Unfortunately, CEDM as a new modality is yet widely available in many other medical centers or breast cancer screening facilities in the U.S. and/or across the world limiting its broad clinical impacts.

F. Gao, T. Wu, and J. Li are with the Industrial Engineering Program at School of Computing, Informatics, and Decision Systems Engineering, Arizona State University, Tempe, AZ 85281, USA. (Emails: fgao16@asu.edu; teresa.wu@asu.edu; jli09@asu.edu).

B. Zheng is with School of Electrical and Computer Engineering, College of Engineering, University of Oklahoma, Norman, OK 73019, USA. (Email: bin.zheng-1@ou.edu).

L. Ruan and D. Shang are with The First Affiliated Hospital of Medical School of Zhejiang University, Hangzhou, China. (Emails: ruanlx@126.com; shdesh@aliyun.com).

B. Patel is with the Department of Radiology, Mayo Clinic in Arizona, Scottsdale, AZ 85259, USA. (Email: patel.bhavika@mayo.edu).

In clinical breast imaging (US, MRI, DM), reading and interpreting the images remains a difficult task for radiologists. Currently, breast cancer screening has high false positive recall rate (i.e., $\geq 10\%$). Computer-aided detection (CADe) and diagnosis (CADx) schemes [13]-[16] have been developed and demonstrated the clinical potentials to be used as “the second reader” to help improve radiologists’ performance in the diagnosis (including DM, US and MRI). In order to overcome the limitation of lower accessibility to CEDM systems and help radiologists more accurately conduct the diagnosis, this research proposes the development and validation of a new CADx scheme, termed Shallow-Deep Convolutional Neural Network (SD-CNN). SD-CNN combines image processing and machine learning techniques to improve the malignancy diagnosis using DM by taking advantages of information available from the CEDM.

CNN is a feed-forward artificial neural network that has been successfully implemented in the broad computer vision areas for decades [17][18]. As it evolves, different CNN models have been developed and implemented. The large amount of computational resource and devices available in recent years make the training of CNN with large number of layers (namely, the deep CNN) possible. Applying deep CNNs in image recognition was probably first discovered in ImageNet competition [19] back in 2012. Since then, it has become a popular model for various applications ranging from natural language processing, image segmentation to medical imaging analysis [20][21]. The main power of a deep CNN lies in the tremendous trainable parameters in different layers [22][23]. These are used to extract discriminative features at different level of abstraction [20]. However, training a deep CNN often requires a large number of labeled training data, which may not be easily available in medical imaging applications. Secondly, training a deep CNN requires massive computational resources, as well as rigorous research in architecture design and hyper-parameters tuning. To address these challenges, a promising solution is transfer learning, that is, a deep CNN model is pre-trained followed by a task-specific parameter fine-tuning process. The pre-trained models are established by experienced researchers using publicly labeled image datasets. For a specific task, the model is often treated as a feature generator to extract features describing the images from abstract level to detailed levels. One can then develop classification models (SVMs, ANNs, etc.) using those features. Promising results have been reported in several medical applications, such as chest pathology identification [24], breast mass detection and classification [25], just to name a few. While exciting, earlier CNN models such as AlexNet [26], GoogLeNet [27] and VGGNet [28] are known to suffer from gradient vanishing when the number of layers increases significantly. A newer model, ResNet [29] with a “short-cut” architecture is recently proposed to address the issue. The imaging competition results show the ResNet outperforms other CNN models by at least 44% in classification accuracy.

The potentials CNN brings to medical imaging research are not limited to deep CNN for imaging feature extraction. A second area that medical research can benefit is indeed from

shallow CNN (less number of layers) for image restoration/reconstruction. Here an image is divided into a number of smaller patches fed into a shallow CNN (e.g., 4-layer CNN in this research) as the input and the output is a restored/reconstructed image. The CNN is trained to learn the non-linear mapping between the input and output images. It is believed that the CNNs also have the ability to de-noise the images, thus improving signal-to-noise ratio of the images. Several successful applications have been reported in using shallow CNN to reconstruct images including MR imaging (MRI), positron emission tomography (PET) imaging [30], ultra-high-field (7T) MR imaging [31] and low-dose/high-dose CT imaging [32].

Motivated by this two-fold applicability of CNN, this research proposes a Shallow-Deep CNN (SD-CNN) as a new CAD scheme to tackle a unique problem stemmed from the novel imaging modality-CEDM, for breast cancer diagnosis. Our first hypothesis is that applying a deep CNN to CEDM is capable of taking advantage of recombined imaging for improved breast lesion classification due to the contribution from the tumor functional image features. Second, in order to expand the advantages of CEDM imaging modality to the regular DM modality, we hypothesize that a shallow CNN is capable to discover the nonlinear mapping between LE and recombined images to render the “virtual” recombined images. As a result, traditional DM can be enriched with the “virtual” recombined images. The objective of this study is to validate these two hypotheses by using a unique study procedure and two imaging datasets of both CEDM and DM images. The details of the study procedures and experimental results are reported in the following section of this paper.

II. MATERIALS

In this research, two separate institutional datasets are used, which include a dataset acquired from tertiary medical center (Mayo Clinic Arizona), and a dataset acquired from the hospital housed at Zhejiang University, China.

A. Institutional Dataset I (Mayo Clinic Arizona):

Based on Institutional Review Board (IRB) approved study and data collection protocol, we reviewed CEDM examinations performed using the Hologic Imaging system (Bedford, MA, USA) between August 2014 and December 2015. All patients undertaken CEDM had a BI-RADS (Breast Imaging Reporting and Data Systems) [34] rating of 4 and 5 in their original DM screening images. Due to the detection of highly suspicious breast lesions, CEDM was offered as an adjunct test to biopsy in a clinical trial environment. All CEDM tests were performed prior to the biopsies. In summary, the patient cohort in this clinical trial had the following criteria: 1) the diagnostic mammogram was rated BI-RADS 4 or 5, and 2) histopathology test result was available from surgical or image-guided biopsy. We limited the cohort to BIRADS 4 and 5 lesions because the analysis required the gold standard of lesion pathology. 49 cases were identified that met the above inclusion criteria, which include 23 benign and 26 cancer biopsy-proven lesions. We analyzed one lesion per patient. If a patient had multiple

enhancing lesions, the annotating radiologist used the largest lesion to ensure best feature selection. In CEDM, there are cranial-caudal (CC) and mediolateral-oblique (MLO) views for both LE and recombined images. Fig. 1 illustrates the example views on the LE and recombined images, respectively.

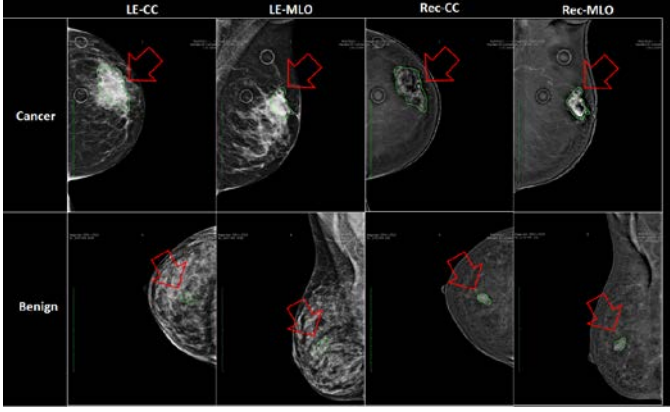


Fig. 1. Example of breast images (Cancer and Benign) for LE and recombined (Rec) images with 2 views (CC and MLO) (Lesions are highlighted with green circle).

For the 49 cases, all CEDM images with DICOM format were de-identified and transferred from the clinical PACS to a research database and loaded into the open source image processing tool OsiriX (OsiriX foundation, Geneva, Switzerland) [35]. DICOM images were anonymized and prepared for blinded reading by a radiologist. A fellowship trained breast radiologist with over 8 years of imaging experience interpreted the mammogram independently and used the OsiriX tool to outline lesion contours. Contours were drawn on recombined images (both CC and MLO views) for each patient on recombined images. These contours were then cloned onto LE images. All lesions were visible on both view CC and MLO views. This information is further used in the imaging pre-processing (see details in methodology section). Some examples LE and recombined images are shown in Figure 1. As observed, LE images are not as easy as recombined images to visualize the lesions for both cancerous and benign cases.

B. Institutional Dataset II (First Affiliated Hospital of Medical School of Zhejiang University):

This dataset was obtained from our collaborators at Zhejiang University, China. During the collecting process, we followed the healthcare privacy policy in China and obtained patient's approval of academic usage. All the images were performed using the Fujifilm Digital Mammography System, ASPIRE Cristalle (FDR MS-3500), both CC and MLO views are available. A total 69 subjects were selected and for each subject, one suspicious region of mass was detected by a radiologist, a biopsy test was conducted afterward to determine whether it is benign or cancer. Among all these 69 subjects, 49 were cancers and 20 were benign. For each subject, the suspicious region was marked by experienced radiologist in yellow rectangle on both CC and MLO views. All cancer subjects are with Elston-Ellis modification of Scarff-Bloom-Richardson grading system

(ESBR) [33] rating of 2 and 3. Examples are shown in Fig.2.

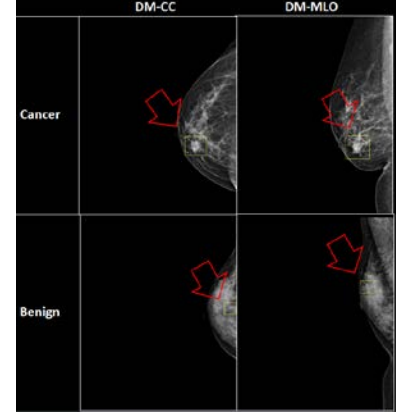


Fig. 2. Example of breast images (Cancer and Benign) for DM images with 2 views (CC and MLO) (Lesions are highlighted with yellow rectangle).

III. METHODOLOGY

To fully explore the advantages of CNNs and CEDM in breast cancer research, a Shallow-Deep CNN (SD-CNN) is proposed (Fig. 3). First, we develop a Shallow-CNN from CEDM to discover the relationships between LE images and recombined images. This Shallow-CNN is then applied to DM to render “virtual” recombined images. Together with DM, a pre-trained Deep-CNN is introduced for feature extraction followed by classification models for diagnosis. Note for CEDM, we can start the workflow with the Deep-CNN directly.

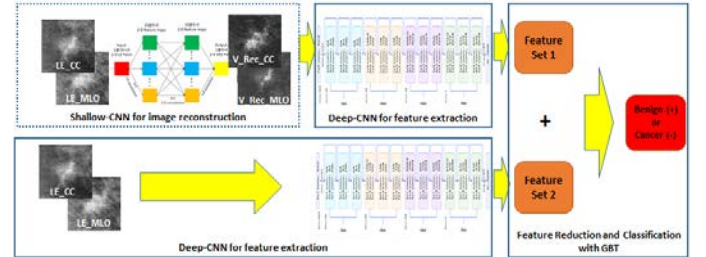


Fig. 3. Architecture of Shallow-Deep CNN

A. Image Pre-processing

Before the Deep-CNN and Shallow-CNN are employed, a four-step imaging pre-processing procedure is launched. First, for each image we identify a minimum-area bounding box that contains the tumor region. Note we have CC and MLO views for DM and we have CC and MLO views for both LE and recombined images for CEDM. As a result, there are two images from DM and four images from CEDM. The bounding box size varies case by case due to different sizes of tumors (ranging from 65×79 to 1490×2137 in this study). Next, an enlarged rectangle that is 1.44 times (1.2 times in width and 1.2 times in height) the size of bounding box is obtained. The enlarged bounding box approach is to include sufficient neighborhood information proved to increase the classification accuracy [36]. In the second step, this ‘enlarged’ rectangle is extracted and saved as one image. The third step is to normalize the image intensity to be between 0 and 1 using the max-min normalization. In the last step, the normalized images are resized to 224×224 to fully take advantage of pre-trained ResNet model.

B. Shallow-CNN: Virtual Image Rendering

Inspired by the biological processes [4], CNNs use a variation of multilayer perceptions designed to require minimal preprocessing. Individual neurons respond to stimuli only in a restricted region of the visual field known as the receptive field. This process is simulated through different layers (convolutional, pooling, fully connected). A CNN's capability is hidden behind the large amount trainable parameters which can be learned iteratively through gradient descent algorithms. In this research, a 4-layer CNN (Fig. 4) is implemented to model the latent relationship between the LE images and recombined images. The model is then used to render “virtual” recombined images from DM images.

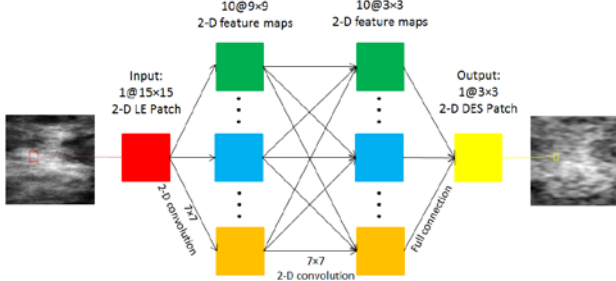


Fig. 4. Architecture of 4-layer shallow-CNN for “virtual” recombined image rendering

C. Deep-CNN: Feature Generation

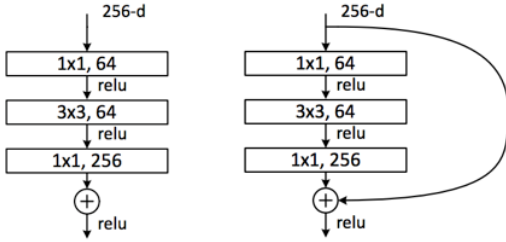


Fig. 5. Building blocks for traditional CNNs (left) and ResNet (right) [29]

ResNet [29] is a pre-trained deep convolutional network developed in 2015 with a revolutionary architecture using the “short-cut” concept in the building block. As seen in Fig. 5, the output of building blocks takes both final classification results and the initial inputs (the short-cut) when updating the parameters. As a result, it outperforms traditional deep-CNNs which are known to suffer from higher testing error as gradient tends to vanish as the number of layers increases [29]. ResNet has different versions with 50, 101 and 152 layers but all based on the same building blocks. In the ImageNet competition, ResNet-50, ResNet-101 and ResNet-152 have comparable performance (top 5 error: 5.25% vs. 4.60% vs. 4.49%), but with quite different numbers of parameter (0.85M vs. 1.7M vs. 25.5M). For the consideration of balance between computation efficiency and accuracy, especially for the limited computation resources, we adopt ResNet-50 in this research.

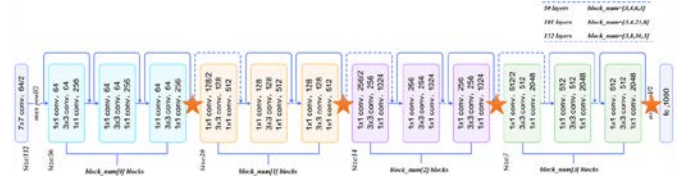


Fig. 6. Architecture of ResNet [37] (Red star are placed in layers where features are extracted; Dotted shortcuts increase feature dimensions by zero-padding; based on the output dimension of building blocks, the ResNet is divided into 4 different building blocks (BBs), they are shown with different colors in the figure (BB_1: blue (Fig. 5 Right), BB_2: orange, BB_3: purple, BB_4: green). Different version of ResNets vary in the number of BBs, for instance, the 50-layer version ResNet has 3 BB_1s, 4 BB_2s, 6 BB_3s and 3 BB_4s).

In general, ResNet consists of four types of buildings blocks. The CNN structures and the number of features for each block are shown in Fig. 6. We mark them with different colors. For simplicity, let blue for block type 1, orange for block type 2, purple for block type 3 and green for block type 3. ResNet-50 is defined as [3, 4, 6, 3] meaning that it has 3 type 1 blocks, 4 type 2 blocks, 6 type 3 blocks and 3 type 4 blocks. The output features are extracted from the final layer of each block type, that is, layer 10, 22, 40 and 49. Since we have no prior knowledge about the feature performance, we decide to take the features from all four layers (10, 22, 40 and 49) for feature selection and classification model development. The number of features extracted from each layer is listed in Table I.

Layer #	10	22	40	49
# of features	256	512	1024	2048

D. Feature Selection and Classification

Boosting is a machine learning ensemble meta-algorithm aiming to reduce bias and variance [38]. It converts weak learners to strong ones by weighing each training sample inverse correlated to performance of previous weak learners. Gradient boosting tree (GBT) is one of the most powerful boosting ensemble decision trees used in regression and classification tasks [39]. It builds the model in a stage-wise fashion, and it generalizes them by allowing optimization of an arbitrary differentiable loss function. The nature of GBT makes it robust to overfitting by measuring the criterion it used when splitting the tree nodes. In addition, it provides the importance of each feature in the regression/classification which can be easily adopted for feature selection. In this research, the number of features are at least 256 (layer 10 from one view) and up to 8196 (layer 49 for both CC and MLO views). We decide to develop a GBT model to reduce the feature dimensions by setting thresholds of feature importance, followed by another GBT for classification of benign versus cancer.

IV. EXPERIMENTS AND RESULTS

The overall objective of this research is to demonstrate the clinical utility of our novel SD-CNN approach for breast cancer diagnosis. To do so, we conduct two sets of experiments. The first experiment is to validate the values from recombined images for improved breast cancer diagnosis. Deep CNN,

ResNet is applied. The second experiment is to investigate the feasibility of applying SD-CNN to enrich the traditional DM to improve the diagnosis.

A. Experiment I: Validating the Improved Accuracy in Breast Cancer Diagnosis on CEDM using Deep-CNN

The workflow of our first experiment is shown in Fig. 7. Using 49 CEDM cases collected from Mayo Clinic Arizona, we first conduct the experiments using LE from CEDM images. For each subject in the dataset, LE images (both CC and MLO views) are processed through pre-processing procedure described in Section III.A, after which 2 patches (224×224) are extracted. They are fed into the pre-trained ResNet. To explore the capability of describing tumors, features from different layers are extracted and evaluated separately. The features are first reduced through GBT based on the feature importance (threshold=0.01, number of features after reduction for different layers can be found in Table III). A second GBT is then implemented with the reduced feature set to classify the case as cancer vs. benign. The procedures are implemented with a python library named “sklearn”. Model settings such as loss function, learning rate, max_depth are default. Different settings to prevent the model from overfitting are used, for instance: we set maximum depth of individual tree to be 3 and use early stopping strategy.

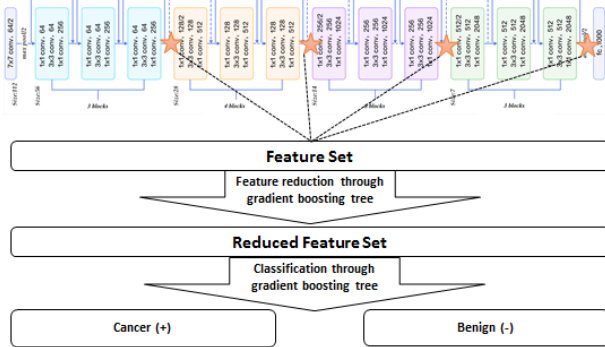


Fig. 7. Workflow of Experiment I

Next, we study the added values from recombined images for improved diagnosis. Specifically, CC and MLO view from recombined images are fed into the same pre-processing and feature generating procedure. The combination of LE and recombined image features are used in the classification model. Performance is measured based on leave-one-out cross validation (due to the limited size of training dataset, leave-one-out cross validation is used here to make fully use of the dataset for training) using accuracy (Acc.), sensitivity (Sen.) and specificity (Sep.). The results are shown in Table II. We observe that the best performing model using LE features provides 0.86 accuracy (Sen.: 0.82, Spe.: 0.90). With additional features from recombined image, the model accuracy improves to 0.90 (Sen.: 0.89, Spe.: 0.90).

TABLE II
CLASSIFICATION PERFORMANCE OF EXPERIMENT USING LE IMAGING VS. LE+RECOMBINED IMAGING

Layer	LE image		LE+recombined image	
	Acc. (Sen., Spe.)	Features after reduction	Acc. (Sen., Spe.)	Features after reduction
10	0.83 (0.89, 0.76)	7	0.87 (0.93, 0.81)	18
22	0.83 (0.85, 0.81)	15	0.85 (0.83, 0.87)	26
40	0.85 (0.85, 0.86)	15	0.89 (0.88, 0.90)	28
49	0.86 (0.82, 0.90)	25	0.90 (0.89, 0.90)	42

We take the best performing model as an example, to explore the features contributing to the classification model. A total of 8192 features from layer 49 are extracted and 42 features are retained after the feature reduction procedure. As introduced in methodology section, the feature’s importance score can be measured through calculating the total impurity reduced by using this feature when building the ensemble trees. Table III summarizes the importance scores for features from different source. (The scores are normalized by dividing individual score with summation of all scores, making the summation to be 100%). From this table, we can get some intuitive insight about the contributions from the recombined images. Among all the 42 features, 25 are from LE images, they contribute 67.13% of the impurity reduction, and the remaining 17 features are from recombined images, the total contribution of these features are 32.87%, and these features help improve the accuracy of breast cancer diagnosis from 0.86 to 0.90. This initial success motivates us to conduct the second set of experiment discussed in the next section.

TABLE III
CONTRIBUTION OF FEATURES FROM DIFFERENT IMAGE SOURCES

Image Source	Number of features	Contribution of impurity reduction
LE image	25	67.13%
Recombined image	17	32.87%

B. Experiment II: Validating the Value of “Virtual” Recombined Imaging in Breast Cancer Diagnosis on DM Using SD-CNN

The improved performance by adding the features from recombined images motivates us to study the feasibility of constructing a “virtual” recombined image from DM images.

Here we first develop a 4-layer shallow CNN that can learn the nonlinear mapping between these the LE and recombined images using the same 49 CEDM dataset. Specifically, by randomly extracting 5000 pair of training samples within masked tumor from each LE (input) and recombined image (output), a training dataset of 245,000 (49×5000) samples is generated. The input samples for the CNN are 15×15 patches from LE images. The output samples for the CNN are the corresponding 3×3 patches from recombined image which is centered in the same position as the LE image. The input and output samples are fed into the CNN framework implemented with package of “Keras”. The CNN has 2 hidden layers, with 10

7*7 filters in each layer. There are a total of 5K trainable parameters through backpropagation with mini-batch gradient decent algorithm to increase learning speed. Batch size is set to be 128. The learning rate is set to be 0.01, ReLu activation function is used in all layers except the output layer, where activation function is not used. Other parameters are set to be default value provided by “Keras” package. Finally, with the trained CNN and patches extracted from available modality, we can construct a “virtual” recombined image by assembling predicted patches into a whole image. For illustration purpose, we choose four samples to demonstrate the resulting “virtual” recombined images vs. the true recombined images (Fig. 8). As seen, the abstract features (e.g., shape) and some details of the tumor from true recombined images are restored by the “virtual” recombined images.

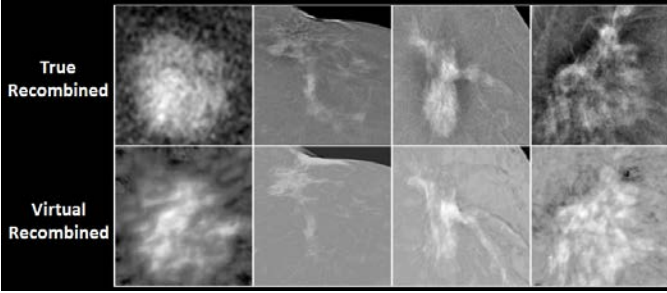


Fig. 8. Sample images of true recombined image and its corresponding virtual recombined in dataset I

With this trained shallow-CNN, we used the 69 DM cases from Zhejiang University to render the “virtual” recombined images. Specifically, for each subject, we slide the 15×15 window from left to right, top to bottom (step size = 1) in DM image, to get the input patches. The input patches are fed into the trained 4-layer CNN, from which we get the predicted virtual recombined image patches (3×3) as outputs. The small patches are placed at the same position as their corresponding input patches in the “virtual” recombined images. For the position with overlapping pixels, the values are replaced with mean value for all overlapping pixels. At last, the “virtual” recombined images are rendered. Fig. 9 illustrates some example DM images and their corresponding “virtual” recombined images. One clinical advantage of recombined image is it filters out dense tissues which often lead to false positive diagnosis. The “virtual” recombined images preserve this advantage. Specifically, as seen in Fig. 9, for each cancer or benign tumor, large portion of surrounding dense tissues are excluded from DM images, while the core region is retained (left two cases in Fig. 9). For the benign case on the rightmost, as the suspicious mass is mainly composed of dense tissue, it is entirely filtered out. We conclude this visual checking is promising and we set to conduct the second set of experiments.

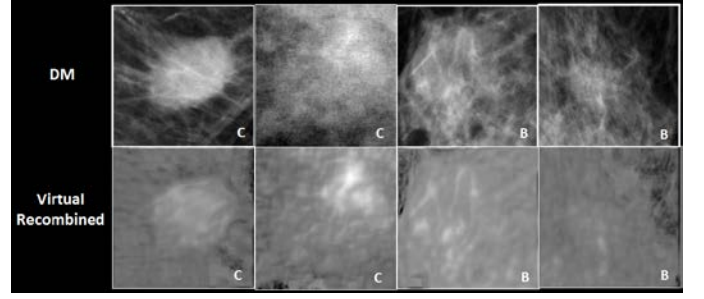


Fig. 9. Sample images of DM in dataset II and its corresponding “virtual” recombined (Two cases on left are Cancer (C), two cases on right are benign (B))

Following the same procedure as the first experiment, we take the ResNet pre-trained and test on the DM and “virtual” recombined images together. Specifically, ResNet is used for feature extraction followed by the GBT feature reduction and GBT ensemble classifiers. The parameter settings for GBT is further tuned since the training dataset is slightly imbalanced (benign: cancer = 29: 40). The training weights for benign and cancer are set to be 1 and 0.72, the learning rate is set to be 0.01. Other parameter settings remain the same. Based on leave-one-out cross validation, the mean performance of each fold of features from different layers is reported in Table IV.

TABLE IV
CLASSIFICATION PERFORMANCE FOR USING DM FEATURE ALONE AND USING FEATURES FROM DM AND “VIRTUAL” RECOMBINED

Layer	DM		DM+ “Virtual” recombined	
	Acc. (Sen., Spe.)	Features after reduction	Acc. (Sen., Spe.)	Features after reduction
10	0.78 (0.88, 0.65)	49	0.84 (0.90, 0.75)	29
22	0.83 (0.82, 0.85)	39	0.87 (0.88, 0.85)	53
40	0.86 (0.94, 0.75)	70	0.86 (0.92, 0.80)	68
49	0.91 (0.96, 0.85)	35	0.95 (0.98, 0.90)	43

As seen in Table IV, the use of “virtual” recombined imaging features significantly improves the performances on accuracy, sensitivity and specificity. Taking the 49 layer as an example, using DM provides the accuracy of 0.91 (Sen: 0.96, Spe: 0.85), and the “virtual” recombined images provides the accuracy of 0.95 (Sen: 0.98, Spe: 0.90). Both sensitivity and specificity are improved after adding the features from the “virtual” recombined images. Following the same procedure as experiment I, we further explore the features selected for the classification modeling to assess the contributions from the “virtual” recombined images. Again, a total of 8192 features from layer 49 are extracted and 43 features are retained after the feature reduction procedure. Table V summarizes the importance score for each feature. Among all the 43 features, 21 are obtained from DM images, they contribute 10.89% of the impurity reduction, and the remaining 22 features are from “virtual” recombined images, the total contribution of these features are 89.11%, and these features help improve the accuracy of breast cancer diagnosis, compared with the experiment with only DM images. We contend the

contributions from “virtual” recombined images are even more significantly than that from the true recombined images. Both the classification model performance (Table IV) and feature contributions (Table V) indicate the importance of the “virtual” recombined images for the diagnosis.

TABLE V
CONTRIBUTION OF FEATURES FROM DIFFERENT IMAGE SOURCES

Image Source	Number of features	Contribution of impurity reduction
DM	21	10.89%
“virtual” recombined image	22	89.11%

V. DISCUSSION AND CONCLUSION

Differentiating benign cases from malignant lesions is one of the remaining challenges of breast cancer diagnosis. In this study, we propose a SD-CNN (Shallow-Deep CNN) to study the two-fold applicability of CNN to improve the breast cancer diagnosis.

One contribution of this study is to investigate the advantages of recombined images from CEDM in helping the diagnosis of breast lesions using a Deep-CNN method. CEDM is a promising imaging modality providing information from standard DM combined with enhancement characteristics related to neoangiogenesis (similar to MRI). Based on our review of literature, no existing study has investigated the extent of CEDM imaging potentials using the deep-CNN. Using the state-of-art pre-trained ResNet as a feature generator for classification modeling, our experiment shows the features from LE images can achieve accuracy of 0.86 with sensitivity of 0.82 and specificity of 0.90, adding the recombined imaging features, model performance improves to accuracy of 0.90 with sensitivity of 0.89 and specificity of 0.90.

Our second contribution lies in addressing the limited accessibility of CEDM and developing SD-CNN to improve the breast cancer diagnosis using DM in general. This the first study to develop a 4 layer shallow-CNN to discover the nonlinear association between LE and recombined images from CEDM. The 4-layer shallow-CNN can be applied to render “virtual” recombined images from DM images to fully take advantage of the CEDM in improved breast cancer diagnosis. Our experiment on 69 DM dataset using the same pre-trained ResNet achieves accuracy of 0.91 with sensitivity of 0.96 and specificity of 0.85. With the “virtual” recombined imaging features, the model performance is improved significantly to accuracy of 0.95 with sensitivity of 0.98 and specificity of 0.90.

While promising, there is room for future work. First of all, the pre-trained ResNet is a black-box feature generator, the features extracted may not be easy to be interpreted by the physicians. It is our intention to discover possible clinical interpretations from the features as one of our future tasks. For example, as the ResNet goes deeper, the initial layers of the features may represent the raw imaging characteristics as the first order statistics, the deeper layer of the features may represent the morphological characteristics (e.g., shape). This is yet to be explored.

REFERENCES

- [1] http://www.breastcancer.org/symptoms/understand_bc/statistics
- [2] Rosenquist, C.J. and K.K. Lindfors, Screening mammography beginning at age 40 years. *Cancer*, 1998. 82(11): p. 2235-2240.
- [3] Berg, W.A., Zhang, Z., Lehrer, D., et al, “Detection of breast cancer with addition of annual screening ultrasound or a single screening MRI to mammography in women with elevated breast cancer risk,” *JAMA*. 307, 1394-1404 (2012).
- [4] Elmore, J.G., et al., Screening for breast cancer. *Jama*, 2005. 293(10): p. 1245-56.
- [5] Kerlikowske, K., et al., Performance of screening mammography among women with and without a first-degree relative with breast cancer. *Ann Intern Med*, 2000. 133(11): p. 855-63.
- [6] Kuhl, C.K., et al., Breast MR imaging screening in 192 women proved or suspected to be carriers of a breast cancer susceptibility gene: preliminary results. *Radiology*, 2000. 215(1): p. 267-79.
- [7] Warner, E., et al., Surveillance of BRCA1 and BRCA2 mutation carriers with magnetic resonance imaging, ultrasound, mammography, and clinical breast examination. *Jama*, 2004. 292(11): p. 1317-25.
- [8] Patel, Bhavika K., Richard J. Gray, and Barbara A. Pockaj. "Potential Cost Savings of Contrast-Enhanced Digital Mammography." *American Journal of Roentgenology* 208.6 (2017): W231-W237.
- [9] Fallenberg, E. M., et al. "Contrast-enhanced spectral mammography versus MRI: initial results in the detection of breast cancer and assessment of tumour size." *European radiology* 24.1 (2014): 256-264.
- [10] Cheung YC, Lin YC, Wan YL, Yeow KM, Huang PC, Lo YF, Tsai HP, Ueng SH, Chang CJ. Diagnostic performance of dual-energy contrast-enhanced subtracted mammography in dense breasts compared to mammography alone: interobserver blind-reading analysis. *European radiology*. 2014 Oct 1;24(10):2394-403.
- [11] Luczyńska E, Heinze-Paluchowska S, Dyczek S, Blecharz P, Rys J, Reinfuss M. Contrast-enhanced spectral mammography: comparison with conventional mammography and histopathology in 152 women. *Korean journal of radiology*. 2014 Dec 1;15(6):689-96.
- [12] Gillman J, Toth HK, Moy L. The role of dynamic contrast-enhanced screening breast MRI in populations at increased risk for breast cancer. *Women's Health*. 2014 Nov;10(6):609-22.
- [13] M. Tan, J. Pu, and B. Zheng. Reduction of false-positive recalls using a computerized mam-mographic image feature analysis scheme. *Physics in medicine and biology*, 59(15):4357, 2014.
- [14] M.Z. Do Nascimento, A.S. Martins, L.A. Neves, R.P. Ramos, E.L. Flores, and G.A. Carrijo. Classification of masses in mammographic image using wavelet domain features and polynomialclassi_er. *Expert Systems with Applications*, 40(15):6213{6221, 2013.
- [15] C. Muramatsu, T. Hara, T. Endo, and H. Fujita. Breast mass classification on mammograms using radial local ternary patterns. *Computers in biology and medicine*, 72:43{53, 2016.
- [16] Gao, Fei, et al. "3D small structure detection in medical image using texture analysis." *Engineering in Medicine and Biology Society (EMBC), 2016 IEEE 38th Annual International Conference of the IEEE*, 2016.
- [17] Y. LeCun, L. Bottou, Y. Bengio, and P. Haffner, “Gradient-based learning applied to document recognition,” *Proceedings of the IEEE*, vol. 86, no. 11, pp. 2278–2324, 1998.
- [18] Y. LeCun, Y. Bengio, and G. Hinton, “Deep learning,” *Nature*, vol. 521, no. 7553, pp. 436–444, 2015.
- [19] Russakovsky, Olga, et al. "Imagenet large scale visual recognition challenge." *International Journal of Computer Vision* 115.3 (2015): 211-252.
- [20] Tajbakhsh, Nima, et al. "Convolutional neural networks for medical image analysis: Full training or fine tuning?." *IEEE transactions on medical imaging* 35.5 (2016): 1299-1312.
- [21] Cha, Kenny H., et al. "Urinary bladder segmentation in CT urography using deep - learning convolutional neural network and level sets." *Medical physics* 43.4 (2016): 1882-1896.
- [22] M. D. Zeiler and R. Fergus, “Visualizing and understanding convolutional networks,” in *Computer Vision—ECCV 2014*. Springer, 2014, pp. 818–833.
- [23] D. Eigen, J. Rolfe, R. Fergus, and Y. LeCun, “Understanding deep architectures using a recursive convolutional network,” *arXiv preprint arXiv:1312.1847*, 201
- [24] Bar, Yaniv, et al. "Deep learning with non-medical training used for chest pathology identification." *Proc. SPIE*. Vol. 9414. 2015.

- [25] Samala, Ravi K., et al. "Mass detection in digital breast tomosynthesis: Deep convolutional neural network with transfer learning from mammography." *Medical physics* 43.12 (2016): 6654-6666
- [26] Krizhevsky, Alex, Ilya Sutskever, and Geoffrey E. Hinton. "Imagenet classification with deep convolutional neural networks." *Advances in neural information processing systems*. 2012.
- [27] K. Simonyan and A. Zisserman. Very deep convolutional networks for large-scale image recognition. In *ICLR*, 2015
- [28] C. Szegedy, W. Liu, Y. Jia, P. Sermanet, S. Reed, D. Anguelov, D. Erhan, V. Vanhoucke, and A. Rabinovich. Going deeper with convolutions. In *CVPR*, 2015
- [29] He, Kaiming, et al. "Deep residual learning for image recognition." *Proceedings of the IEEE conference on computer vision and pattern recognition*. 2016.
- [30] Li, Rongjian, et al. "Deep learning based imaging data completion for improved brain disease diagnosis." *International Conference on Medical Image Computing and Computer-Assisted Intervention*. Springer, Cham, 2014.
- [31] Bahrami, Khosro, et al. "Reconstruction of 7T-like images from 3T MRI." *IEEE transactions on medical imaging* 35.9 (2016): 2085-2097.
- [32] Chen, Hu, et al. "Low-Dose CT with a Residual Encoder-Decoder Convolutional Neural Network (RED-CNN)." *arXiv preprint arXiv:1702.00288* (2017).
- [33] Rakha, Emad A., et al. "Prognostic significance of Nottingham histologic grade in invasive breast carcinoma." *Journal of clinical oncology* 26.19 (2008): 3153-3158.
- [34] D'Orsi CJ, editor. *ACR BI-RADS Atlas: Breast Imaging Reporting and Data System*. 2013.
- [35] Rosset A, Spadola L, Ratib O. OsiriX: an open-source software for navigating in multidimensional DICOM images. *Journal of digital imaging*. 2004 Sep 1;17(3):205-16.
- [36] Lévy D, Jain A (2016) Breast mass classification from mammograms using deep convolutional neural networks. *arXiv:1612.00542*
- [37] http://book.paddlepaddle.org/03.image_classification/
- [38] Bauer, Eric, and Ron Kohavi. "An empirical comparison of voting classification algorithms: Bagging, boosting, and variants." *Machine learning* 36.1 (1999): 105-139.
- [39] Breiman, Leo. *Arcing the edge*. Technical Report 486, Statistics Department, University of California at Berkeley, 1997.